

Holocene atmospheric circulation in the central North Pacific: a new terrestrial diatom and $\delta^{18}\text{O}$ dataset from the Aleutian Islands

Hannah L Bailey ^{a,b,c,*}, Darrell S Kaufman ^d, Hilary J Sloane ^e, Alun L Hubbard ^f, Andrew CG Henderson ^g, Melanie J Leng ^{e,h}, Hanno Meyer ^b, and Jeffrey M Welker ^{a,c}

^a Department of Biological Sciences, University of Alaska Anchorage, Anchorage, AK 99508, USA

^b Alfred Wegener Institute for Polar and Marine Research, Potsdam 14473, Germany

^c Department of Ecology and Genetics, University of Oulu, Oulu, Finland

^d School of Earth Sciences & Environmental Sustainability, Northern Arizona University, Flagstaff, AZ 86011, USA

^e NERC Isotope Geosciences Facility, British Geological Survey, Nottingham NG12 5GG, UK

^f Centre for Arctic Gas Hydrate, Environment and Climate, Department of Geology, UiT The Arctic University of Norway, 9037 Tromsø, Norway

^g School of Geography, Politics and Sociology, Newcastle University, Newcastle-upon-Tyne, NE7 1RU, UK

^h Centre for Environmental Geochemistry, School of Biosciences, University of Nottingham, Loughborough, LE12 5RD, UK

* *Corresponding author.* Current address and affiliation: Hannah.Bailey@oulu.fi (University of Oulu)

Key words: Holocene; Paleoclimate; North Pacific; Limnology; Stable Isotopes; Diatoms

Highlights:

- New Holocene oxygen isotope record from the Aleutian Islands
- Diatom $\delta^{18}\text{O}$ reflects shifts in synoptic-scale atmospheric circulation
- Warmer/wetter early-mid Holocene, cooler/drier after 4.5 ka
- Enhanced winter circulation corresponds to Holocene glacier advances
- Current environmental changes unprecedented within past 9.6 ka

Abstract

The North Pacific is a zone of cyclogenesis that modulates synoptic-scale atmospheric circulation, yet there is a paucity of instrumental and paleoclimate data to fully constrain its long-term state and variability. We present the first Holocene oxygen isotope record ($\delta^{18}\text{O}_{\text{diatom}}$) from the Aleutian Islands, using siliceous diatoms preserved in Heart Lake on Adak Island (51.85° N, 176.69° W). This study builds on previous work demonstrating that Heart Lake sedimentary $\delta^{18}\text{O}_{\text{diatom}}$ values record the $\delta^{18}\text{O}$ signal of precipitation, and correlate significantly with atmospheric circulation indices over the past century. We apply this empirical relationship to interpret a new 9.6 ka $\delta^{18}\text{O}_{\text{diatom}}$ record from the same lake, supported by diatom assemblage analysis. Our results demonstrate distinct shifts in the prevailing trajectory of storm systems that drove spatially heterogeneous patterns of moisture delivery and climate across the region. During the early-mid Holocene, a warmer/wetter climate prevailed due to a predominantly westerly Aleutian Low that enhanced advection of warm ^{18}O -enriched Pacific moisture to Adak, and culminated in a $\delta^{18}\text{O}_{\text{diatom}}$ maxima (33.3 ‰) at 7.6 ka during the Holocene Thermal Maximum. After 4.5 ka, relatively lower $\delta^{18}\text{O}_{\text{diatom}}$ indicates cooler/drier conditions associated with enhanced northerly circulation that persisted into the 21st century. Our analysis is consistent with surface climate conditions inferred from a suite of terrestrial and marine climate-proxy records. This new Holocene dataset bridges the gap in an expanding regional network of paleoisotope studies, and provides a fresh assessment of the complex spatial patterns of Holocene climate across Beringia and the atmospheric forces driving them.

1. Introduction

Numerous paleoenvironmental studies now contribute to a global synthesis and understanding of Holocene climate change over the past 11.7 ka [Mayewski *et al.* 2004; Marcott *et al.* 2013; Rehfeld *et al.* 2018]. By comparing common trends between individual proxy records, these studies provide a means to infer the timing, scale, and spatial extent of major Holocene climatic features. These include stepwise climate transitions, intervals exceeding twentieth century warmth, and the low-frequency behaviour and modes of natural climate variability. At broad (i.e. global) spatial and temporal scales these trends are relatively coherent and unambiguous, yet at finer spatial scales, climate variability is more pronounced due to local and regional factors. Such variability is highlighted in two recent paleoclimate syntheses focused on west and eastern Beringia – the region extending from northeast Siberia to northwest Canada (Fig. 1a) [Brooks *et al.* 2015; Kaufman *et al.* 2016]. While general circulation models (GCM) typically emphasise insolation as the key driver of millennial-scale Holocene climate change [Renssen *et al.* 2009], these compilations indicate a more complex and spatially heterogeneous climate evolution than implied by linear insolation forcing alone. For example, major climatic features previously considered ubiquitous, such as a prominent Holocene thermal maximum (HTM) [Kaufman *et al.* 2004], are now recognised to be spatially asynchronous across this vast region [Kaufman *et al.* 2016]. Moreover, existing terrestrial water isotope records are also shown to be ambiguous and contradictory during the Holocene [Kaufman *et al.* 2016], and the most recent suite of model-data comparisons reveal significant mismatches between simulated and reconstructed Holocene temperatures in Alaska [Zhang *et al.* 2017].

At the synoptic scale, Beringia is located within the main centre of influence of the Aleutian Low; one of the most dominant ocean-atmospheric systems in the Northern Hemisphere and of global climate significance [Rodionov *et al.* 2007]. However, virtually all available terrestrial paleoclimate data are restricted to mainland Alaska and eastern Russia

[Sundqvist *et al.* 2014; Brooks *et al.* 2015; Kaufman *et al.* 2016], and compared to lower latitude regions, paleoisotope reconstructions are sparse [Kaufman *et al.* 2016]. This partly reflects a lack of base-line water isotope measurements for constraining the regional water isotope cycle [e.g. Welker, 2000; Anderson *et al.* 2016], as well as a paucity of lake core studies with continuous sequences of carbonate-rich sediments – or suitable alternatives – for isotopic analysis. Hence, to elucidate past and future climate in this region, there is an outstanding requirement for greater spatial coverage of highly resolved and accurately dated paleoclimate datasets, as well as an empirical-based understanding of the atmospheric and environmental controls driving them.

To address this, we present the first Holocene oxygen isotope record from the Aleutian Islands in south west Alaska. Our isotope measurements derive from siliceous diatoms ($\delta^{18}\text{O}_{\text{diatom}}$) preserved in the sediments of Heart Lake, on Adak Island (Fig. 1b), and are supported by diatom assemblage analysis of the same sedimentary sequence. We build on earlier work by Bailey *et al.* [2015] who demonstrate that Heart Lake $\delta^{18}\text{O}_{\text{diatom}}$ values correlate significantly with North Pacific climate indices over the past hundred years ($r = 0.43$; $p < 0.02$, $n = 28$). Here, we apply this empirically-derived understanding to interpret new $\delta^{18}\text{O}_{\text{diatom}}$ data from a longer Heart Lake sediment core which extends back to 9.6 ka. The primary aims are to: (1) investigate the forcing and response of this remote region to a warming climate system as it transitioned from the last glacial period; (2) develop a Holocene reconstruction of North Pacific atmospheric circulation; and (3) bridge the gap in the regional network of proxy records to synthesise and assess complex spatio-temporal patterns of natural climate variability across Beringia.

2. Regional Setting

Heart Lake is a small ($\sim 0.25 \text{ km}^2$), freshwater through-flow system on Adak Island in the central North Pacific (51.85° N , 176.69° W) (Fig. 1c). The island is volcanic and forms part

of the 1900-km-long Aleutian archipelago extending from mainland Alaska to the Russian-Kamchatka Peninsula. The lake watershed area is $\sim 8 \text{ km}^2$ and is situated in low-relief hills surrounded by mountainous terrain (Fig. 1c). There is a single lake basin with a maximum depth of 8 m. One stream inflows from two larger lakes and a small outflow channel drains to the Bering Sea $\sim 2 \text{ km}$ to the west. Lake volume is $\sim 8 \times 10^5 \text{ m}^3$ and water retention is an estimated two weeks, based on the available stream gauge inflow data [TDX, 2013]. Inspection of available satellite imagery reveals that Heart Lake freezes over in winter and this ice surface remains into spring [USGS, 2017].

Adak Island has a mild maritime climate compared to mainland Alaska and is strongly affected by persistent fog and light rain in the summer, and frequent storms and strong winds during winter [Rodionov *et al.* 2007]. Mean annual air temperature is 4.3°C , and mean winter (December–February) and summer (June–August) values are 1.0°C and 9.0°C , respectively (1949–2016) [NOAA, 2017]. Mean December and July precipitation is 163 mm and 71 mm, respectively (Fig. 1d) [NOAA, 2017]. Of the total 1.3 m annual precipitation, $\sim 75\%$ (1.0 m) falls from September to February.

The regional climate reflects the configuration of large scale atmospheric–ocean systems, namely the Aleutian Low: a synoptic-scale feature of mean low sea level pressure (SLP) and the leading driver of North Pacific climate [Mock *et al.* 1998]. When the Aleutian Low is ‘weak’, storms tend to track north over the central Aleutian Islands (Fig. 2a); when the pressure system is ‘strong’, storms track south of the Aleutians and into the Gulf of Alaska (Fig. 2b) [Mock *et al.* 1998; Rodionov *et al.* 2007]. These circulation patterns vary on interannual to decadal timescales and induce characteristic climate responses that are well expressed in coupled modes of the North Pacific Index (NPI) and the Pacific Decadal Oscillation (PDO) [Trenberth and Hurrell, 1994; Mantua *et al.* 1997]. Typically, a strong Aleutian Low ($- \text{NPI}/+ \text{PDO}$) will induce positive sea surface temperatures (SST), surface air temperatures (SAT), and precipitation anomalies in the Gulf of Alaska and negative

anomalies in the central North Pacific, with contrary conditions during a weak Aleutian Low (+NPI/-PDO) (see Supplementary Fig.1).

3. Materials and Methods

3.1. Sediment and water recovery

Sediment cores and bottom lake water samples were recovered from Heart Lake during the summers of 2009 and 2010. A Garmin GPS sonar was used to survey its bathymetry and revealed a single basin with a maximum depth of 8 m, surrounded by a shallow platform < 2 m deep (see Supplementary Figure 2). Coring sites were selected adjacent to the deepest part of the basin at a depth of 7.6 m. Seven sediment cores were extracted using percussion and hand-held gravity coring devices operated from a floating platform. Bottom lake water samples were collected *in situ* at the sediment-water interface during gravity coring. Following core extraction the water was directly siphoned from the corer and sealed in 50 ml vials, ensuring no head space. Sediment cores were then split lengthways, packaged, and shipped with water samples to Northern Arizona University where they were stored at 4 °C until they were sub-sampled and analyzed. Our study focuses on the longest percussion core (10-AS-1D; 5.9 m) and two accompanying surface gravity cores (09-AS-1A, 0.81 m; and 09-AS-1B, 0.44 m). For a detailed description of the sediment core's lithostratigraphy, see *Krawiec et al.* [2013].

3.2. Chronology

The composite age model for 10-AS-1D and 09-AS-1A is presented in a separate paper devoted to the tephrostratigraphy and radiometric dating of the Heart Lake sedimentary sequence [*Krawiec et al.* 2013] (Supplementary Fig. 3a). In summary, a Monte Carlo approach was employed to model the age-depth relation of 16 macrofossil AMS radiocarbon (¹⁴C) dates, together with a peak in recent ²³⁹+²⁴⁰Pu activity and the age of the sediment-water

interface (2009 AD) [Krawiec *et al.* 2013]. Tephrostratigraphy was used to independently cross check the accuracy of the chronology, whereby the ages of down core tephra horizons from Heart Lake were compared with tephra ages from nearby Andrew Lake and previously published outcrop studies [Krawiec *et al.* 2013]. The chronology for surface core 09-AS-1B derives from radiometric dating of ^{210}Pb , ^{226}Ra , ^{137}Cs and ^{241}Am by direct gamma assay on 14 dried sediment samples from the upper core section [Bailey *et al.* 2015] (Supplementary Fig. 3b). The cores were cross-correlated using a prominent tephra horizon found in all three sedimentary sequences [Krawiec *et al.* 2013; Bailey *et al.* 2015]. All ages herein are expressed as thousands of calendar years (ka) prior to 1950 AD, where 1 ka = 1000 cal yr BP.

3.3. Stable isotope analyses

A total of 147 sediment samples were processed for $\delta^{18}\text{O}_{\text{diatom}}$ analysis. These samples range in age from 9.6 ka (587 cm depth) to 2009 AD, and are sub-/decadally resolved for the most recent 1500 years and at centennial resolution thereafter. From the 5.9 m-long core 10-AS-1D, 1 cm³ of sediment was extracted at 7 cm intervals from the base (587 cm) to the top of the core. This was the optimal sampling resolution to avoid tephra layers which could potentially cause contamination issues [Lamb *et al.* 2007]. The surface cores 09-AS-1A and 09-AS-1B were both sampled in contiguous 0.5 cm increments. This detail was used to capture sub-decadal changes in $\delta^{18}\text{O}_{\text{diatom}}$ over the past century for direct comparison with instrumental datasets [see Bailey *et al.* 2015]

Sediment samples were prepared using a hybrid process of chemical digestion, sieving, and heavy liquid separation adapted from Morley *et al.* [2004]. To remove organic and carbonate material, samples were treated with 30% H_2O_2 at 90°C until reactions ceased, before using 5 % HCl at ambient temperature. Samples were then centrifuged in sodium polytungstate ($3\text{Na}_2\text{WO}_4 \cdot 9\text{WO}_3 \cdot \text{H}_2\text{O}$) (SPT) heavy liquid at 2500 rpm for 20 minutes, resulting in the separation and suspension of diatoms from the heavier detritus. This

procedure was repeated three times for each sample using specific gravities of 2.50, 2.30 and 2.25 g ml⁻¹. After the final SPT separation, samples were washed five times in ultrapure water (UPW) at 1500 rpm for 5 minutes and vacuum filtered through a 3 µm cellulose nitrate membrane to remove potential clay minerals and/or broken diatom fragments. The < 3 µm fraction was discarded as it was too small (< 1 mg) to be analyzed and, upon further inspection under a light microscope, contained only small broken diatom fragments and detritus. The remaining samples were treated with a final stage of 30 % H₂O₂ at 60 °C for one week to ensure no traces of organic matter remained.

Purified diatom samples were analyzed for δ¹⁸O_{diatom} using the stepwise fluorination method [Leng and Sloane, 2008] at the NERC Isotope Geosciences Laboratory in Keyworth, UK. The outer hydrous layer of the diatom was removed in a pre-fluorination stage using a BrF₅ reagent at low temperature [Leclerc and Labeyrie, 1987]. This was followed by a full reaction at high temperature to liberate oxygen that was converted to CO₂ [Clayton and Mayeda, 1963] and measured for δ¹⁸O_{diatom} using a MAT 253 dual-inlet mass spectrometer. Replicate analyses indicate an analytical reproducibility of ±0.19 ‰ (1σ) for the samples, and ±0.30 ‰ (1σ) for the diatom standard BFC_{mod}. All δ¹⁸O values were converted to the Vienna Standard Mean Ocean Water (VSMOW) scale using the BFC_{mod} standard for calibration.

Two Heart Lake water samples were measured for their oxygen and hydrogen (δD) isotope composition using a Thermo-Finnigan Deltaplus XL gas mass spectrometer at the Colorado Plateau Stable Isotope Laboratory, Northern Arizona University, USA. Analytical precision on internal working standards was ±0.1 ‰ for δ¹⁸O and ±1 ‰ for δD. All values are reported here in per mil (‰) relative to VSMOW.

3.3.1. Contamination assessment

All purified diatom samples (n = 147) were visually inspected for contamination using an OLYMPUS BX40 light microscope. Thirty samples were selected down-core and further

inspected using a Hitachi S-4700 field emission scanning electron microscope (SEM). In addition, fourier transform infrared spectroscopy (FTIR) was applied to assess the chemical composition and sample purity of 16 diatom samples from core 10-AS-1D [Swann and Patwardham, 2011]. These samples, together with the BFC_{mod} diatom standard, were analyzed using FTIR at the British Geological Survey in Keyworth, UK [Bailey et al. 2014]. FTIR analyses of all purified diatom isotope samples measured (n=16) indicate peaks corresponding to the BFC_{mod} standard, known to represent clean, fossilised diatomite (Supplementary Fig. 4). Spectral deviation from the standard would indicate additional compounds and contamination by non-diatom components [Swann and Patwardhan, 2011]; peaks centred at ~450 cm⁻¹, ~800 cm⁻¹ and ~1100 cm⁻¹ confirm pure silica and the integrity of our diatom isotope samples [Bailey et al. 2014].

3.4. Diatom assemblage analysis

Fifty-seven sub-samples of the purified diatom material used for $\delta^{18}\text{O}_{\text{diatom}}$ analysis were retained for diatom species analysis. These include 33 samples selected at c. 13 cm intervals from AS-10-1D, and 24 samples at a contiguous 0.5 cm resolution from AS-09-1B. Diatom slides were prepared on a hot plate using Naphrax[®] mounting medium. A minimum of 300 diatom frustules per sample were counted along transects at x1000 magnification, under an OLYMPUS BX40 light microscope. Taxonomic identification was based on classifications in Camburn and Charles [2000] and Krammer and Lange-Bertalot [1986–1991].

Following diatom identification, species counts were converted to percentage abundance and evaluated using the software package Tilia (v.2.0.41) [Grimm, 2015]. For diatom zone demarcation, a constrained incremental sum-of-squares cluster analysis (CONISS) [Grimm, 1987] was applied to all dominant taxa with a relative abundance >5 % in at least one sample. To quantitatively assess the down core trends in diatom assemblages, a principal components analysis (PCA) [ter Braak and Prentice, 1988] was applied to a

correlation matrix based on the dominant (>5 %) diatom species in all 57 samples. The analysis was performed on untransformed percentage data using the program C2 (v.1.7.6) [Juggins, 2014].

4. Results

4.1. Diatom flora

Diatom frustules are well preserved in all samples and show no sign of valve dissolution. The flora is diverse and a total of 155 different freshwater diatom species were identified. Of these, 11 species account for > 90 % of all diatoms present in all samples. These include species belonging to the genera *Aulacoseira*, *Cyclotella*, *Rossithidium*, and small fragilarioid taxa (consisting of the genera *Fragilaria*, *Pseudostaurosira*, *Staurosira*, *Stauroforma*, and *Staurosirella*). Species with an abundance ≥ 5 % in at least one stratigraphic level are presented (Fig. 3), and the record is divided into four zones based on the CONISS dendrogram: *Zone 1* (9.6–8.6 ka; 587–452 cm), *Zone 2* (8.6–4.4 ka; 452–352 cm), *Zone 3* (4.4 ka–1860 AD; 352–13.25 cm), and *Zone 4* (1860–2009 AD; 13.25–0 cm). Species are grouped into one of three habitat types (planktonic, benthic, or facultatively planktonic) based on classifications by Spaulding *et al.* [2017] (Fig. 3).

Diatom *Zone 1* (587–452 cm; ca. 9.6–8.6 ka) is dominated by *Staurosirella pinnata* (33 %), *Cyclotella ocellata* (18 %), and other small fragilarioid taxa (60 %) (Fig. 3). By ca. 9.0 ka the abundance of *S. pinnata* decreases to 10 % and the planktonic species *Cyclotella rossii* (10–30 %), *Aulacoseira subarctica* (4–25 %) and *Cyclotella ocellata* (5–14 %) are more dominant. Some of the small benthic species all show slight increases in abundance at this time, including *Psammothidium levanderi* (9 %) and *Achnantheidium minutissimum* (6%), albeit at a low relative abundance.

In *Zone 2* (452–352 cm; ca. 8.6–4.4 ka) the planktonic species *C. ocellata*, *A. subarctica*, and *C. rossii* begin to dominate the assemblage (Fig. 3). Collectively these

species reach a maximum abundance of 75 % between 8.5–7.6 ka; a time when small benthic and facultatively planktonic taxa are at their overall lowest Holocene abundances (0–5 %). Increases in abundances of *Rossithidium pussilum* and other small fragilarioid taxa occur *ca.* 7.6 and 6.8 ka, concurrent with a decrease in planktonic taxa (Fig. 3). After *ca.* 5.0 ka, the abundance of planktonic species gradually decrease, paralleled by increasing abundance of facultatively planktonic taxa.

At the onset of Zone 3 (352–13.25 cm; 4.4 ka–1860 AD) a large increase in the facultatively planktonic taxa is paralleled by declines in planktonic taxa (Fig. 3). Collectively, the small fragilarioid taxa make up ~80 % of the assemblages in this zone and several species attain their maximum Holocene abundance, including *S. pinnata* at 4.2 ka (39 %) and *Staurosira construens* at 3.8 ka (28 %). In contrast, planktonic species decline from a mean abundance of 55 % in Zone 2, to 5 % in Zone 3. Only *Tabellaria flocculosa* shows relatively little change in abundance from Zone 2, remaining at ~4%. Of the benthic taxa, *Stauroforma exiguiiformis* and *R. pusillum* are also present in high abundances throughout Zone 3, with the former attaining a maximum Holocene abundance of 26 % at *ca.* 2.2 ka.

In Zone 4 (13.25–0 cm; *ca.* 1860–2009 AD) the small fragilarioid taxa continue to dominate the assemblage, comprising ~75 % of the total assemblage *ca.* 1910 AD (Fig. 3). After this time, the abundance of facultatively planktonic taxa steadily decreases as the benthic and planktonic species increase. After *ca.* 1970 AD, the numbers of *A. subarctica* decreases substantially, such that only a few individual frustules were counted per sample.

Stratigraphic changes in diatom flora are captured in the first two PCA components, which collectively account for 71 % of the total assemblage variance (Fig. 4). Additional eigenvectors defined by the PCA (3–5) were not considered given they explain progressively lower proportions of the total variance ($\lambda_3=0.108$, $\lambda_4=0.059$, $\lambda_5=0.038$). PCA 1 represents 57 % of total variance and correlates to the planktonic species at the positive extreme, and the facultatively planktonic species at the negative extreme. PCA 2 accounts for 14 % of total

variance, and correlates to the small fragilarioid taxa (Fig. 4). The Holocene succession of diatom communities in Heart Lake is further illustrated by the time-series of the 54 sample scores on PCA axis 1 (Fig. 3).

4.2. Oxygen isotopes

Holocene $\delta^{18}\text{O}_{\text{diatom}}$ values vary between 24.6 ‰ (1805 AD) and 33.3 ‰ (7.6 ka) ($\bar{x} = 29.7$ ‰, $n = 137$) (Fig. 5) with a range of ± 8.7 ‰ that is appreciably greater than the standard deviation of all samples (± 0.19 ‰) and diatom standards (± 0.30 ‰) measured. The base of the Heart Lake sediment core has a $\delta^{18}\text{O}_{\text{diatom}}$ value of 29.7 ‰ at 9.6 ka, and values steadily increase to the maximum Holocene value of 33.3 ‰ at *ca.* 7.6 ka (Fig. 5). After 4.9 ka $\delta^{18}\text{O}_{\text{diatom}}$ becomes progressively lower until *ca.* 3.5 ka (27.8 ‰) where values remain stable at ~ 29 –30 ‰ until *ca.* 1.0 ka. After *ca.* 1.0 ka, $\delta^{18}\text{O}_{\text{diatom}}$ exhibits high variability to lower values *ca.* 1250–1340 AD and 1430–1525 AD, and after 1640 AD there is a shift to overall lower $\delta^{18}\text{O}_{\text{diatom}}$ values, including the Holocene minimum $\delta^{18}\text{O}_{\text{diatom}}$ value of 24.6 ‰ at 1805 AD. The $\delta^{18}\text{O}_{\text{diatom}}$ values then slightly increase between 1805–1903 AD, before decreasing to the present day (29.8 ‰) (Fig. 5). Using the sub-division age of 4.2 ka for the mid-late Holocene boundary [Walker *et al.* 2012], late Holocene $\delta^{18}\text{O}_{\text{diatom}}$ is significantly ($p < 0.001$) lower than in the early–mid Holocene.

5. Discussion

5.1. Oxygen isotope paleohydrology and paleoclimatology

Oxygen isotope ratios measured in precipitation ($\delta^{18}\text{O}_{\text{p}}$) at Adak airport (1962–67, 1972–73; $n = 60$) indicate mean annual precipitation-weighted $\delta^{18}\text{O}_{\text{p}}$ is -8.8 ‰, with small seasonal differences between January (-9.4 ‰) and July (-8.9 ‰) [IAEA/WMO, 2017]. The correspondence between Heart Lake water $\delta^{18}\text{O}$ and the local and global meteoric water lines confirms that (1) Heart Lake water $\delta^{18}\text{O}$ reflects local precipitation, and (2) evaporative

effects influencing precipitation and lake water $\delta^{18}\text{O}$ are minimal with no isotopic enrichment (Fig. 6). Specifically, the two Heart Lake bottom water ($\delta^{18}\text{O}_{\text{water}}$) samples collected in summer 2009 and 2010 ($\bar{x} = -9.5\text{‰}$) are directly comparable, within error, to the long term winter and spring $\delta^{18}\text{O}_{\text{P}}$ values from Adak airport. These data indicate the lake water budget is dominated by winter and spring precipitation (i.e. snowfall and melt) similar to many lakes and streams across Alaska [Clegg and Hu, 2010; Lachniet et al. 2016; Vachula et al. 2017].

There is no correlation between mean monthly $\delta^{18}\text{O}_{\text{P}}$ and SAT ($r = 0.15$, $n = 72$) or precipitation amount ($r = 0.03$, $n = 72$) at Adak airport. Instead, Bailey et al. [2015] found that Adak Island $\delta^{18}\text{O}_{\text{P}}$ values are primarily controlled by the moisture source and trajectory of local precipitating storm systems. Specifically, winters with intensified Aleutian Low circulation are characterized by precipitation with significantly ($p < 0.05$) lower than mean $\delta^{18}\text{O}_{\text{P}}$ values. These variations are explained by systematic shifts in the central foci of the Aleutian Low; when the SLP minimum is near Adak (strong Aleutian Low), polar air masses are drawn south and advect water vapor and precipitation that is relatively depleted in ^{18}O , along with lower-than-average winter temperatures and increased snowfall (Fig. 2b) [Rodionov et al. 2007; Bailey et al. 2015]. In contrast, a weakened and westerly displaced Aleutian Low increases the southerly Pacific moisture flux to Adak via an enhanced south-westerly storm track (Fig. 2a) [Rodionov et al. 2007]. These systems carry warm ^{18}O -enriched moisture, and bring higher-than-average temperatures and increased precipitation to Adak Island [Bailey et al. 2015].

$\delta^{18}\text{O}_{\text{diatom}}$ is controlled by several environmental parameters which depend on local hydrology, climate, and the seasonality of diatom growth [Barker et al. 2001; Rioual et al. 2001; Jones et al. 2004; Rosqvist et al. 2004; Leng and Barker, 2006; Schiff et al. 2009; Mackay et al. 2011; Meyer et al. 2015; Chaplignin et al. 2016]. Previous work by Bailey et al. [2015] showed that the surface core $\delta^{18}\text{O}_{\text{diatom}}$ record from Heart Lake correlates significantly with the winter NPI during the instrumental period (1900–2009 AD) ($r = 0.43$, $p < 0.02$, $n =$

28). This positive relationship confirms that Heart Lake diatoms precipitate their silica frustule in isotopic equilibrium with the lake water in which they grow [Labeyrie, 1974; Leclerc and Labeyrie, 1987], independent of size or species-related vital effects [Bailey *et al.* 2014]. During the spring thaw, it is evident that winter season precipitation ($\delta^{18}\text{O}_\text{p}$) enters Heart Lake coincident with onset of the spring diatom bloom. A limited component of residual summer growth might be expected, but bulk $\delta^{18}\text{O}_\text{diatom}$ analysis is weighted toward the main period of diatom growth in spring [Leng *et al.* 2001; Bailey *et al.* 2014]. Under the assumption that similar climatic controls on $\delta^{18}\text{O}_\text{p}$ prevailed before 1900 AD, we use this extended $\delta^{18}\text{O}_\text{diatom}$ record as a proxy for atmospheric circulation throughout the Holocene.

5.2. Holocene environmental history of Adak Island

5.2.1. Early-mid Holocene, 9.6 – 4.4 ka

Adak Island, along with the Aleutian chain, was glaciated during the last glacial maximum, though there are few chronological constraints on the onset and pattern of ice retreat [Coats, 1956; Bradley, 1948; Fraser and Snyder, 1959; Black, 1976]. At Heart Lake, percussion coring ceased at a depth of 587 cm without penetrating bedrock or till, indicating the catchment deglaciated prior to 9.6 ka.

From 9.6–9.0 ka, the dominance of fragilarioid and other small benthic taxa reflect a temperate oligotrophic shallow lake with an extensive littoral zone. These pioneering taxa dominate polar to subpolar and mountainous tundra lakes [Lotter and Bigler, 2000; Rühland *et al.* 2003; Hausmann and Pienitz, 2009; Devlin and Finkelstein, 2011] and their presence suggests a relatively short growth season with cool air temperatures [Smol *et al.* 2005; Rühland *et al.* 2008; Hausmann and Pienitz, 2009]. Cool/dry conditions at this time are further supported by low concentrations of biogenic silica (BSi) and organic matter (OM) in

nearby Andrew Lake [Krawiec and Kaufman, 2014] and the dominance of *Salix* and *Empetrum* in northern Adak [Heusser, 1978].

Heart Lake was increasingly colonized by planktonic diatoms between 9.3–4.4 ka (Fig. 3). Of these, *A. subarctica* is common across Arctic and subarctic zones, and typically shows pronounced periodicity with the spring maximum in non-stratified lakes [Bradbury et al. 2002; Baier et al. 2004; Rioual et al. 2007; Gibson et al. 2003; Solovieva et al. 2015]. It is a heavily silicified species, forming colonies that require turbulence-induced suspension to remain within the photic zone [Rühland et al. 2008; Lotter et al. 2010], and indicates persistent strong seasonal winds, together with associated turbulent water mixing and nutrient upwelling [Wang et al. 2008; Andrén et al. 2015; Solovieva et al. 2015]. In contrast, *Cyclotella* species have a competitive advantage over the heavily silicified *A. subarctica* during strong stratification [Andrén et al. 2015] and typically bloom after ice-out in subarctic regions [Rühland et al. 2008; Hoff et al. 2015]. In Kamchatka, *Cyclotella* spp. prosper during warmer years [Lepskaya et al. 2010], and are broadly considered warm water indicators due to their recent expansion across Arctic lakes [Smol et al. 2005; Rühland et al. 2008]. Collectively, these early-mid Holocene diatom assemblages reveal a phase of overall high lake mixing and turbidity, reduced lake ice cover, and relatively high Si/P ratios [Interlandi et al. 1999; Rühland et al. 2003; Rioual et al. 2007]. These changes are further summarized by the Holocene time series of PCA 1 sample scores (Fig. 3).

The isotope composition of Heart Lake water was significantly ($p < 0.001$) higher during the early-mid Holocene compared to the late Holocene (Fig. 5), reflecting the prevalence of southerly storms delivering abundant precipitation with higher $\delta^{18}\text{O}$ values [Bailey et al. 2015]. Such warm, southerly winter storms would promote turbulent mixing and limit the development of winter lake ice, thereby extending the open-water growing season and allowing for a spring diatom assemblage dominated by planktonic species (Fig. 3). *Aulacoseira subarctica*, in particular, is abundant in modern lake systems during years

with short, warm winters [Gibson *et al.* 2003; Horn *et al.* 2011]. Elevated pollen percentages of *Cyperaceae* and other wetland species in northern Adak also imply warm/wet conditions at this time [Heusser, 1978] and correspond to higher local lake levels prior to 4.0 ka [Krawiec and Kaufman, 2014]. Peak $\delta^{18}\text{O}_{\text{diatom}}$ (33.3 ‰) suggests maximum Holocene warmth at 7.6 ka, an inference supported by the simultaneous maximum Holocene abundance of the warm water indicator *C. ocellata* [Rühland *et al.* 2008] (Fig. 3).

The $\delta^{18}\text{O}_{\text{diatom}}$ record correlates positively with the time series of PCA 1 scores ($r = 0.48$, $p < 0.001$) and demonstrates that diatom community structure is indirectly connected to climate over millennial timescales. It also indicates that diatom species changes are a natural ecological response to climatically-driven shifts in lake water $\delta^{18}\text{O}$, as reflected in the $\delta^{18}\text{O}_{\text{diatom}}$ record, rather than the converse (i.e. changes in diatom species drive $\delta^{18}\text{O}_{\text{diatom}}$ variation).

5.2.2. Mid-late Holocene, 4.4 ka – present

At around 4.4 ka, a major shift in diatom composition occurred with marked changes from a predominantly planktonic assemblage to the dominance of small fragilarioid and benthic taxa (Fig. 3). During this transition the relatively warm, deep, and well-mixed open-water conditions of the early-mid Holocene (9.6–4.4 ka) gave way to a less turbulent, potentially shallower lake. This transition coincides with a shift to lower $\delta^{18}\text{O}_{\text{diatom}}$ values in the late Holocene, reflecting an increase of isotopically depleted water (i.e. snow and/or ice melt) during the spring thaw [Bailey *et al.*, 2015; Streletskiy *et al.* 2015], and reduced warm, ^{18}O -enriched southerly storms that characterized the early-mid Holocene.

An increase in northerly winds and lower temperatures during the late Holocene would have enhanced formation of winter lake ice, which in turn was insulated and prolonged by increased winter snowfall [Mock *et al.* 1998]. Persistence of lake ice into the spring shortens the aquatic growth season and restricts light penetration into the water column

during the spring bloom, thereby precluding the growth and development of planktonic communities requiring an ice-free lake for photosynthesis and a turbulent, well-mixed water column. Instead, the mid-late Holocene flora at Heart Lake is dominated by fragilarioid species known to colonise benthic and periphytic habitats under lake ice cover [Lotter and Bigler, 2000; Douglas and Smol, 2010; Biskaborn et al. 2016]. These benthic communities would have further benefitted from the absence of competition for nutrients from planktonic diatoms, which do not thrive under ice [Lepskaya et al. 2010; Roberts et al. 2015]. A reduction in turbulent wind-driven lake mixing at this time may have also been responsible for increased benthic production and a simultaneous expansion of the littoral zone and benthic habitat [Bradbury, 1988]. Increased winter precipitation and subsequent spring snow melt would account for the sedimentation increase at 3.8 ka from 0.2 to 0.8 mm/yr [Krawiec and Kaufman, 2014]. This turbidity would have further reduced light penetration into the benthic zone, thereby promoting fragilarioid taxa which thrive under limited light and generally turbid conditions [Lotter and Bigler, 2000; Douglas and Smol, 2010].

The simultaneous changes in diatom species assemblages and $\delta^{18}\text{O}_{\text{diatom}}$ values ca. 4.4 ka reflect numerous factors affecting vertical mixing patterns, availability of resources (e.g. light, nutrients), and thereby the algal production and composition of Heart Lake. These pronounced changes broadly coincided with other paleoenvironmental changes on Adak Island centred ca. 4.4 ka. For example the BSi and inferred chlorophyll-*a* record from nearby Andrew Lake also indicates increased aridity after 4.0 ka [Krawiec and Kaufman, 2014], while reconstructed plant assemblages show a reduction in *Cyperaceae* after ca. 4.5 ka as cooler/drier conditions prevailed over Adak Island [Heusser, 1978].

Between 950 AD and 1200 AD, higher $\delta^{18}\text{O}_{\text{diatom}}$ indicates a transition to overall warmer and wetter conditions on Adak (Fig. 5). A decrease in *Empetrum* vegetation across northern Adak also indicates increased moisture [Heusser, 1978], while Krawiec and Kaufman [2014] interpret sustained low BSi and chlorophyll-*a* content from Andrew Lake as

the stormiest interval on record. Our $\delta^{18}\text{O}_{\text{diatom}}$ values exhibit high variability between 950 and 1900 AD, implying the local climate was also wetter and more variable since 950 AD. These conditions would account for the continued dominance of fragilarioid taxa over this period with unstable lake conditions [Smol *et al.* 2005; Rühland *et al.* 2008; Hausmann and Pienitz, 2009]. Additionally, a peak in sedimentation *ca.* 1.0 ka, attributed to increased storminess [Krawiec and Kaufman, 2014], rendered conditions unfavourable for planktonic diatom species due to increased sediment suspension and reduced light penetration. Unlike numerous diatom assemblage records across the subarctic and Arctic, in Heart Lake there is no major shift toward those taxa favouring longer growing seasons under warming climatic conditions (e.g. *Cyclotella*) [Smol *et al.* 2005]. Conversely, benthic assemblages show an increase after *ca.* 1860 AD (Fig. 3), reflecting an overall strengthening of Aleutian Low circulation since 1900 AD [Trenberth and Hurrell, 1994] and increasingly unstable environmental conditions on Adak Island over the past century. These findings are consistent with observations in North America and Greenland that suggest shifts in *Cyclotella* abundances are more closely related to lake mixing, water clarity and resource availability, rather than direct temperature effects [Saros and Anderson, 2015].

5.3. Regional paleoenvironmental context

Our $\delta^{18}\text{O}_{\text{diatom}}$ reconstruction reveals distinct shifts in the prevailing trajectory of storm systems delivering moisture to Adak Island. The primary trends suggest a relatively weak and westerly positioned Aleutian Low during the early-mid Holocene (9.7–4.5 ka), with a strengthening eastward shift after *ca.* 4.5 ka (Fig. 5). Based on 21st century observations, typical climatic responses to a weakened Aleutian Low are: (1) a weakening of Pacific mid-latitude storm tracks; (2) increased meridional flow to the central-western Bering Sea; and (3) reduced winter sea surface heat loss in the central-western Bering Sea and enhanced heat loss from the Okhotsk Sea [Mock *et al.* 1998; Rodionov *et al.* 2007]. Under this synoptic regime

the following conditions would be anticipated in regional paleoclimate records: (1) a reduction in winter storms and precipitation in the Gulf of Alaska region; (2) positive precipitation and temperature anomalies in the central-western Aleutian Islands; and (3) SST warming and reduced winter sea ice extent in the central-western Bering Sea and contrary conditions in the Okhotsk Sea.

In support of this synoptic-scale picture, vegetation and lake-level reconstructions provide independent evidence for considerably drier winter conditions in eastern Beringia during the early-mid Holocene [Anderson *et al.* 2005; RS Anderson *et al.*, 2006; Zander *et al.* 2013]. For example, numerous lakes in southern Alaska and the Yukon record lower-than-present water levels during the early Holocene until *ca.* 8 ka [Kaufman *et al.* 2016], reflecting a combination of higher summer temperatures and lower winter precipitation. Furthermore, an inferred decrease in frequency and intensity of winter storms steered into the Gulf of Alaska accounts for marked episodes of glacial retreat at this time [Solomina *et al.* 2015], driven by reduced winter snowfall/accumulation and negative net mass balance.

The SST patterns associated with a weakened wintertime Aleutian Low are also evident during the early-mid Holocene. Relatively warm early Holocene SSTs are documented from the western Bering Sea [Max *et al.* 2012], reflecting a persistently negative phase of the PDO during the early-mid Holocene and an increase in Pacific storms tracking into the region [Rodionov *et al.* 2007]. In the Okhotsk Sea, alkenone-derived SST estimates correspond well with Heart Lake $\delta^{18}\text{O}_{\text{diatom}}$ between *ca.* 9.6–5.0 ka (Fig. 7), whereby higher $\delta^{18}\text{O}_{\text{diatom}}$ and an inferred weak Aleutian Low corresponds to lower early-mid Holocene SSTs [Max *et al.* 2012]. This relationship conforms to modern northerly geostrophic wind anomalies during a weakened and westward displaced Aleutian Low that cool and enhance polynya growth in the Okhotsk Sea [Itaki and Ikahara, 2004; Harada *et al.* 2014]. Specifically, warm (cold) winter SSTs in the Bering Sea (Okhotsk Sea) presently occur when the Aleutian Low is shifted west and the Siberian High dominates over central western

Siberia [Rodionov *et al.* 2007]. These anti-correlated trends also manifest in sea-ice anomalies on weekly to monthly time-scales during the 21st century [Cavalieri and Parkinson, 1987] and are linked to the east–west migration of the Siberian High and Aleutian Low.

We find independent support for the Holocene migration of the Siberian High from the Pechora Lake $\delta^{18}\text{O}$ record in northern Kamchatka [Hammarlund *et al.* 2015] (Fig. 7). A north-eastward shift of the Siberian High, concurrent with a strong and eastward shifted Aleutian Low, is linked to periods of increased winter snow contributions to Pechora Lake and overall lower $\delta^{18}\text{O}$ values [Hammarlund *et al.* 2015]. The coherency of abrupt and persistent change between the Heart and Pechora Lake $\delta^{18}\text{O}$ records between 9.6–3.5 ka provides convincing evidence that the Aleutian Low–Siberian High system prevailed throughout the early-mid Holocene (Fig. 7). Moreover, we propose that the synchronous west-east migration of these systems may have been partially responsible for the non-linear and heterogeneous climatic patterns reconstructed across east and west Beringia at this time [Brooks *et al.* 2015; Kaufman *et al.* 2016].

Maximum values of $\delta^{18}\text{O}_{\text{diatom}}$ in Heart Lake at 7.6 ka broadly coincide with the northern high-latitude (65 °N) summer insolation maxima *ca.* 8.0 ka (Fig. 7) [Berger and Loutre 1991]. Significantly ($p < 0.001$) higher $\delta^{18}\text{O}_{\text{diatom}}$ in Heart Lake – relative to both the modern (1900 AD–present) and long-term (9.6 ka–present) mean $\delta^{18}\text{O}_{\text{diatom}}$ – implies a HTM in the central Aleutian Islands at 7.6 ka characterized by persistently weak Aleutian Low circulation, and coincident with maximum abundances of warm water indicator species [Smol *et al.* 2005] (Fig. 3). Similarly, a Holocene SST maximum is evident *ca.* 7.5 ka in both the northwest Pacific [Minoshima *et al.* 2007] and the subarctic North Pacific [Harada *et al.* 2014], and from GCMs which indicate maximum SATs and SSTs in the Bering Sea and Aleutian Islands *ca.* 7.0–8.0 ka [Renssen *et al.* 2012]. In southern Kamchatka, the majority of paleoenvironmental records demonstrate a HTM *ca.* 7.0–5.3 ka [Brooks *et al.* 2015], consistent with warm temperatures across eastern Beringia [Kaufman *et al.* 2016]. These

results contrast with previous paleoclimate studies from Alaska and the northwest Pacific that identify an earlier HTM at *ca.* 11.3–9.1 ka [Kaufman *et al.* 2004; Max *et al.* 2012]. Such uncertainty in these early Holocene warming patterns is highlighted by Zhang *et al.* [2017] who found large discrepancies between modelled and reconstructed Holocene temperatures across Alaska. Hence, it is difficult to fully constrain the timing of the HTM in the central Aleutian Islands, particularly given that our record does not extend the full Holocene epoch coupled with a paucity of local alternative studies.

Simultaneous shifts in diatom flora and $\delta^{18}\text{O}_{\text{diatom}}$ after the HTM at *ca.* 4.5 ka indicate multiple and inter-related environmental changes that impacted Heart Lake. These pronounced changes coincide with local proxy inferences demonstrating increased aridity under a prevailing northerly circulation pattern [Heusser, 1978; Corbett *et al.* 2010; Krawiec and Kaufman, 2014]. This mid-Holocene perturbation coincides with a return to cooler conditions, increased winter precipitation and extensive glacial advance in Kamchatka [Nazarova *et al.* 2013; Barr and Solomina, 2014; Meyer *et al.* 2015]. Widespread cooling is also evident in eastern Beringia during the late Holocene [Kaufman *et al.* 2016], and mountain glaciers across Alaska advanced between *ca.* 4.5 and 3.0 ka [Solomina *et al.* 2015], in phase with those in Kamchatka and demarking onset of the Neoglacial across Beringia [Savoskul, 1999; Barr and Solomina, 2014]. Though temperature is proposed as the principal control on regional glacier mass balance through the Holocene [Solomina *et al.* 2015], the observed glacial maxima in Alaska are asynchronous with the timing of pronounced cold intervals [Kaufman *et al.* 2016]. Instead, our data suggest the transition to intensified Aleutian Low circulation after 4.5 ka, coincident with declining summer insolation [Berger and Loutre, 1991], drove widespread Neoglacial advance through the combined effect of increased winter snowfall under a generally cooler regime, yielding a marked regional positive mass balance perturbation. In particular, we note during the past millennium three intervals of lower $\delta^{18}\text{O}_{\text{diatom}}$ values between 1275–1350 AD, 1400–1550 AD, and 1700–1850

AD coincide with three well-documented episodes of Little Ice Age (LIA) glacier advance on mainland Alaska (Fig. 5 and 7) [Calkin *et al.* 2001; Solomina *et al.* 2015]. Furthermore, the $\delta^{18}\text{O}_{\text{diatom}}$ minimum at 1805 AD (+24.6 ‰) marks the culmination of regional LIA glacial advance [Barclay *et al.* 2009; Calkin *et al.* 2001; Wiles *et al.* 2004; Solomina *et al.* 2015] (Fig. 5 and 7).

5.4 Coherency of paleoisotope trends

Several paleoisotope records from Alaska have also been interpreted in terms of synoptic-scale changes in atmospheric circulation and inter-comparison with Heart Lake $\delta^{18}\text{O}_{\text{diatom}}$ yields many commonalities and insights [Anderson *et al.* 2005; Fisher *et al.* 2004; 2008; Schiff *et al.* 2009; Jones *et al.* 2014; Hammarlund *et al.* 2015] (Fig. 7). For instance, a strong inverse relationship *ca.* 9.5–4.0 ka is apparent with millennial scale $\delta^{18}\text{O}_{\text{diatom}}$ variations at Mica Lake, in Prince William Sound [Schiff *et al.* 2009] (Fig. 7). Lower Mica Lake $\delta^{18}\text{O}_{\text{diatom}}$ values indicate precipitation delivered by zonal flow under a weak Aleutian Low, whereby precipitating systems are subject to increased rainout as they pass over the Kenai Peninsula and coastal mountain ranges. Conversely, increased meridional flow during a strong Aleutian Low delivers locally sourced moisture from nearby Gulf of Alaska, thereby reducing distillation and isotope depletion in precipitation, thus yielding higher Mica Lake $\delta^{18}\text{O}_{\text{diatom}}$ values [Schiff *et al.* 2009]. The reciprocal relationship between precipitation-inferred $\delta^{18}\text{O}$ values at Heart and Mica Lakes between *ca.* 9.5–4.0 ka conforms to modelling and empirical analyses of spatial patterns of $\delta^{18}\text{O}_{\text{p}}$ [Berkelhammer *et al.* 2012; Bailey *et al.* 2015]. The Horse Trail Fen record from the Kenai lowlands is also comparable to Heart Lake from *ca.* 8.0 ka and demonstrates overall higher $\delta^{18}\text{O}$ values during the early Holocene and reflecting generally weak Aleutian Low circulation [Jones *et al.* 2014]. The only other full Holocene paleoisotope record from eastern Beringia is from the Mount Logan ice core [Fisher *et al.* 2008], which exhibits strong correspondence with the Jellybean [Anderson *et al.* 2005] and

Heart Lake $\delta^{18}\text{O}$ records during the early-mid Holocene (Fig. 7).

Secondary, but notable departures between paleoisotope records are evident during the late Holocene (Fig. 7), some of which can be reconciled by considering the detailed, non-linear complexity of atmospheric circulation. For instance between *ca.* 3.0–1.0 ka Heart Lake $\delta^{18}\text{O}_{\text{diatom}}$ does not exhibit marked excursions to the higher $\delta^{18}\text{O}$ values documented in Mt. Logan, Jellybean and Pechora Lakes, interpreted as an interval of pronounced weak Aleutian Low circulation [Anderson *et al.* 2005; Fisher *et al.* 2008; Hammarlund *et al.* 2015]. At Heart Lake, this period is characterized by $\delta^{18}\text{O}_{\text{diatom}}$ values closer to the Holocene mean (Fig. 7). These differences could reflect prevailing atmospheric patterns characterized by a more southerly displaced western centre of low pressure in the northwest Pacific, which typically results in a higher density of storms being steered into the Gulf of Alaska and eastern Kamchatka Peninsula [Mock *et al.* 1998; Rodionov *et al.* 2007]. Under such conditions, precipitation at Mt. Logan, Jellybean and Pechora Lakes would be relatively ^{18}O -enriched [Berkelhammer *et al.* 2012], whereas Heart Lake would fail to exhibit higher $\delta^{18}\text{O}_{\text{diatom}}$ values since these storm systems would track south of the Aleutian Islands [Rodionov *et al.* 2007].

6. Conclusions

The new datasets and analysis presented here extend modern observations across Alaska and Siberia back through the Holocene to bridge a critical gap in the regional network of proxy-climate records [Sundqvist *et al.* 2014; Brooks *et al.* 2015; Kaufman *et al.* 2016]. Although GCMs typically emphasize insolation as the key driver of Holocene temperature change in Alaska [Renssen *et al.* 2009], we demonstrate a more complex relationship and emphasise the role of moisture availability and transport within the land–atmosphere–ocean system.

The Aleutian Islands straddle a critical zone of cyclogenesis that influences regional temperature and precipitation patterns, including the heat and moisture flux between the

extratropical Pacific and Arctic; hence, the variable modes of atmospheric circulation we identify have a wide reaching global influence through atmospheric-oceanic teleconnections. Our empirically-derived understanding of the drivers and magnitude of these past changes provide a means to contextualise contemporary climate trends, along with their potential future trajectory and impact, across Alaska and the wider North Pacific. Specifically, we demonstrate that Holocene shifts in Aleutian Low circulation directly impacted the net mass balance of south-central Alaska's glaciers and ice fields through temperature and precipitation variability [Solomina *et al.* 2015]. Given that Alaska is currently experiencing a period of intensified Aleutian Low circulation, which should be favorable for glacier *growth*, the widespread and well documented 21st century retreat of glaciers and ice cover [Larsen *et al.* 2015] would now appear to be unprecedented within the context of long-term Holocene environmental change.

7. Acknowledgements

This research was funded by NSF award EAR 0823522, NERC grants IP/1202/1110 and IP/1460/0514, and a NERC CASE award to H.L.B. (NE/I528350/1). The research was further supported by a Lloyds of London Fulbright Fellowship award to H.L.B. during the preparation of this manuscript. We thank Yarrow Axford, Anne Krawiec, Caleb Schiff, and David Vaillencourt for their field assistance. The US Fish and Wildlife Service, Alaska Maritime Natural Wildlife Refuge and CPS Polar services provided logistical support and access for fieldwork on Adak Island.

8. Data availability

Key datasets for this study are available in Supplementary Table 1. All data produced by this study (*will be*) available online at the World Data Center for Paleoclimatology (WDC Paleo)

(<https://www.ncdc.noaa.gov/data-access/paleoclimatology-data>) and in the NERC National
Geoscience Data Centre (NGDC) (<http://www.bgs.ac.uk/services/ngdc/>).

9. References

- Anderson, L., Abbot, M.B., Finney, B.P., and Burns, S.J., (2005), Regional atmospheric
circulation change in the North Pacific during the Holocene inferred from lacustrine
carbonate oxygen isotopes, Yukon Territory, Canada, *Quat. Res.*, 64, 21–35, doi:
10.1016/j.yqres.2005.03.005.
- Anderson, R.S., Hallett, D.J., Berg, E., Jass, R.B., Toney, J.L., De Fontaine, C.S., and
DeVolder, A., (2006), Holocene development of boreal forests and fire regimes on the Kenai
Lowlands of Alaska, *The Holocene*, 16(6), 791–803, doi: 10.1191/0959683606hol966rp.
- Anderson, L., Berkelhammer, M., Barron, J.A., Steinman, B.A., Finney, B.P., and Abbott,
M.B., (2016), Lake oxygen isotopes as recorders of North American Rocky Mountain
hydroclimate: Holocene patterns and variability at multi-decadal to millennial timescales,
Glob. Planet. Change, 137, 131–148, doi: 10.1016/j.gloplacha.2015.12.021.
- Andrén, E., Klimaschewski, A., Self, A. E., Amour, N. S., Andreev, A. A., Bennett, K. D.,
Conley, D.J., Edwards, T.W.D., Solovieva, N., and Hammarlund, D., (2015), Holocene
climate and environmental change in north-eastern Kamchatka (Russian Far East), inferred
from a multi-proxy study of lake sediments, *Global Planet. Change*, 134, 41–54, doi:
10.1016/j.gloplacha.2015.02.013.
- Baier, J., Lücke, A., Negendank, J.F., Schleser, G.H., and Zolitschka, B., (2004), Diatom and
geochemical evidence of mid-to late Holocene climatic changes at Lake Holzmaar, West-
Eifel (Germany), *Quat. Int.*, 113(1), 81–96, doi: 10.1016/S1040-6182(03)00081-8.
- Bailey, H.L., Henderson, A.C.G., Sloane, H.J., Snelling, A., Leng, M.J., and Kaufman, D.S.,

644 (2014), The effects of species on lacustrine $\delta^{18}\text{O}_{\text{diatom}}$ and its implications for environmental
645 reconstructions, *J. Quat. Sci.*, 29, 393–400, doi: 10.1002/jqs.2711.

646 Bailey, H.L., Kaufman, D.S., Henderson, A.C.G., and Leng, M.J., (2015), Synoptic scale
647 controls on the $\delta^{18}\text{O}$ in precipitation across Beringia, *Geophys. Res. Lett.*, 42, 4608–4616,
648 doi: 10.1002/2015GL063983.

649 Barclay, D.J., Wiles, G.C., and Calkin, P.E., (2009), Holocene glacier fluctuations in Alaska,
650 *Quat. Sci. Rev.*, 28, 2034–2048, doi: 10.1016/j.quascirev.2009.01.016.

651 Barker, P.A., Street-Perrott, F.A., Leng, M.J., Greenwood, P.B., Swain, D.L., Perrott, R.A.,
652 Telford, J., and Ficken, K.J., (2001) A 14 ka oxygen isotope record from diatom silica in two
653 alpine tarns on Mt. Kenya, *Science*, 292, 2307–2310, doi: 10.1126/science.1059612.

654 Barr, I.D., and Solomina, O., (2014), Pleistocene and Holocene glacier fluctuations upon the
655 Kamchatka Peninsula, *Glob. Planet Change*, 113, 110–120, doi:
656 10.1016/j.gloplacha.2013.08.005.

657 Berger, A., and Loutre, M.F., (1991), Insolation values for the climate of the last 10 million
658 years, *Quat. Sci. Rev.*, 10, 297–317, doi:10.1016/0277-3791(91)90033-Q.

659 Berkelhammer, M., Stott, L., Yoshimura, K., Johnson, K., and Sinha, A., (2012), Synoptic
660 and mesoscale controls on the isotopic composition of precipitation in the western United
661 States, *Climate Dynamics*, 38 (3-4), 433–454, doi: 10.1007/s00382-011-1262-3.

662 Biskaborn, B.K., Subetto, D.A., Savelieva, L.A., Vakhrameeva, P.S., Hansche, A.,
663 Herzsuh, U., Klemm, J., Heinecke, L., Pestryakova, L.A., Meyer, H., and Kuhn, G.,
664 (2016), Late Quaternary vegetation and lake system dynamics in north-eastern Siberia:
665 Implications for seasonal climate variability, *Quat. Sci. Rev.*, 147, 406–421, doi:
666 10.1016/j.quascirev.2015.08.014.

667 Black, R.F., (1976), Late Quaternary glacial events, Aleutian Islands, Alaska. In:
 668 Easterbrook, D.D., Sibrava, V. (Eds.), Quaternary Glaciations in the Northern Hemisphere.
 669 IUGSUNESCO International Geological Correlations Program, Project 73-1-24. International
 670 Union of Quaternary Research, Bellingham, pp. 285–301.

671 Bradbury, P., Cumming, B., and Laird, K., (2002), A 1500-year record of climatic and
 672 environmental change in Elk Lake, Minnesota III: measures of past primary productivity, *J.*
 673 *Paleolimnol.*, 27(3), 321–340, doi: 10.1023/A:1016035313101.

674 Bradley, C.C., (1948), Geologic notes on Adak Island and the Aleutian chain, Alaska, *Am. J.*
 675 *Sci.*, 246(4), 214-240, doi: 10.2475/ajs.246.4.214.

676 Brooks, S.J., Diekmannb, B., Jones, V.J., and Hammarlund, D., (2015), Holocene
 677 environmental change in Kamchatka: A synopsis, *Glob. Planet Change*, 134, 166–174, doi:
 678 10.1016/j.gloplacha.2015.09.004.

679 Calkin, P.E., Wiles, G.C., and Barclay, D. J., (2001), Holocene coastal glaciation of Alaska,
 680 *Quat. Sci. Rev.*, 20, 449–461, doi: 10.1016/S0277-3791(00)00105-0.

681 Camburn, K.E., and Charles, D.F., (2000), *Diatoms of Low-alkalinity Lakes in the*
 682 *Northeastern United States*, ANSP Special Publication 18. Academy of Natural Sciences of
 683 Philadelphia, Philadelphia.

684 Cavalieri, D.J., and Parkinson, C.L., (1987), On the relationship between atmospheric
 685 circulation and the fluctuations in the sea ice extents of the Bering and Okhotsk Seas, *J.*
 686 *Geophys. Res.*, 92, 7141–7162, doi: 10.1029/JC092iC07p07141.

687 Chaplignin, B., Narancic, B., Meyer, H., and Pienitz, R., (2016), Paleo-environmental
 688 gateways in the eastern Canadian arctic—Recent isotope hydrology and diatom oxygen

isotopes from Nettilling Lake, Baffin Island, Canada, *Quat. Sci. Rev.*, 147, 379–390, doi:
10.1016/j.quascirev.2016.03.028.

Clayton, R.N., and Mayeda, T.K., (1963), The use of bromine pentafluoride in the extraction
of oxygen from oxide and silicates for isotopic analysis, *Geochim. Cosmochim. Acta*, 27, 43–
52, doi: 10.1016/0016-7037(63)90071-1.

Clegg, B.F., and Hu, F.S., (2010), An oxygen-isotope record of Holocene climate change in
south-central Brooks Range, Alaska, *Quat. Sci. Rev.*, 29, 928–939, doi:
10.1016/j.quascirev.2009.12.009.

Coats, R.R., (1956), *Reconnaissance geology of some western Aleutian Islands, Alaska*, US
Geological Survey Bulletin 1028-E, Government Printing Office.

Corbett, D., West, D., and Lefevre, C., (2010), *The People at the End of the World: The
Western Aleutian Project and the Archeology of Shemya Island*, Alaska Anthropological
Association Monograph Series VIII.

Devlin, J.E., and Finkelstein, S.A., (2011), Local physiographic controls on the responses of
Arctic lakes to climate warming in Sirmilik National Park, Nunavut, Canada, *J. Paleolimnol.*,
45(1), 23–39, doi: 10.1007/s10933-010-9477-6.

Douglas, M.S.V., and Smol, J.P., (2010), *Freshwater diatoms as indicators of environmental
change in the High Arctic*, In: Smol, J.P., Stoermer, E.F. (Eds.), *The Diatoms: Application for
the Environmental and Earth Sciences*. Cambridge University Press, Cambridge, pp.
249–266.

Fisher, D.A., Wake, C., Kreutz, K., Yalcin, K., Steig, E., Mayewski, P., Anderson, L., Zheng,
J., Rupper, S., Zdanowicz, C., Demuth, M., Waszkiewicz, M., Dahl-Jensen, D., Goto-Azuma,
K., Bourgeois, J.B., Koerner, R.M., Sekerka, J., Osterberg, E., Abbott, M.B., Finney, B.P.,

712 and Burn, S.J., (2004), Stable isotope records from Mount Logan, Eclipse ice cores and
 713 nearby Jellybean Lake. Water cycle of the North Pacific over 2000 years and over five
 714 vertical kilometres: Sudden shifts and tropical connections, *Geogr. Phys. Quat.*, 58 (2–3),
 715 337–352, doi: 10.7202/013147ar.

716 Fisher, D., Osterberg, E., Dyke, A., Dahl-Jensen, D., Demuth, M., Zdanowicz, C., Bourgeois,
 717 J., Koerner, R.M., Mayewski, P., Wake, C., Kreutz, K., Steig, E., Zheng, J., Yalcin, K., Goto-
 718 Azuma, K., Luckman B., and Rupper, S., (2008), The Mt Logan Holocene-late Wisconsinan
 719 isotope record: tropical Pacific--Yukon connections, *The Holocene*, 18, 667–677, doi:
 720 10.1177/0959683608092236.

721 Fraser, G.D., and Snyder, G.L., (1959), *Geology of southern Adak Island and Kagalska*
 722 *Island, Alaska*, US Geological Survey Bulletin 1028, pp. 371–408.

723 Gibson, C.E., Anderson, N.J., and Haworth, E.Y., (2003), *Aulacoseira subarctica*: taxonomy,
 724 physiology, ecology and palaeoecology, *Eur. J. Phycol.*, 38, 83–101, doi:
 725 10.1080/0967026031000094102.

726 Grimm, E.C., (1987), Coniss - a Fortran-77 program for stratigraphically constrained cluster-
 727 analysis by the method of incremental sum of squares. *Comput. Geosci.*, 13, 13–35.

728 Grimm, E.C., (2015) TILIA software. Version 2.0.41. <https://www.tilait.com/download/>

729 Hammarlund, D., Klimaschewski, A., St. Amour, N.A., Andrén, E., Self, A.E., Solovieva, N.,
 730 Andreev, A.A., Barnekowa, L., and Edwards, T.W.D, (2015), Late Holocene expansion of
 731 Siberian dwarf pine (*Pinus pumila*) in Kamchatka in response to increased snow cover as
 732 inferred from lacustrine oxygen-isotope records, *Glob. Planet. Change*, 134, 91–100, doi:
 733 10.1016/j.gloplacha.2015.04.004.

734 Harada, N., Katsuki, K., Nakagawa, M., Matsumoto, A., Seki, O., Addison, J.A., Finney,
 735 B.P., and Sato, M., (2014), Holocene sea surface temperature and sea ice extent in the
 736 Okhotsk and Bering Seas, *Prog. Oceanogr.*, 126, 242–253, doi:
 737 10.1016/j.pocean.2014.04.017.

738 Hausmann, S., and Pienitz, R., (2009), Seasonal water chemistry and diatom changes in six
 739 boreal lakes of the Laurentian Mountains (Québec, Canada): impacts of climate and timber
 740 harvesting, *Hydrobiologia*, 635(1), 1–14, doi: 10.1007/s10750-009-9855-0.

741 Heusser, C.J., (1978), Post-glacial vegetation on Adak Island, Aleutian Islands, Alaska. *Bull.*
 742 *Torrey Bot. Club.*, 105, 18–23, doi: 10.2307/2484259.

743 Hoff, U., Biskaborn, B.K., Dirksen, V.G., Dirksen, O., Kuhn, G., Meyer, H., Nazarova, L.,
 744 Roth, A., and Diekmann, B., (2015), Holocene environment of Central Kamchatka, Russia:
 745 Implications from a multi-proxy record of Two-Yurts Lake, *Glob. Planet. Change*, 134,
 746 101–117, doi: 10.1016/j.gloplacha.2015.07.011.

747 Horn, H., Paul, L., Horn, W., and Petzoldt, T., (2011), Long-term trends in the diatom
 748 composition of the spring bloom of a German reservoir: is *Aulacoseira subarctica* favoured
 749 by warm winters? *Fresh. Biol.*, 56(12), 2483–2499, doi: 10.1111/j.1365-2427.2011.02674.x.

750 IAEA/WMO, (2017), *Global Network of Isotopes in Precipitation*, The GNIP Database.
 751 Accessible at: <http://www.iaea.org/water>.

752 Interlandi, S.J., Kilham, S.S., and Theriot, E.C., (1999), Responses of phytoplankton to
 753 varied resource availability in large lakes of the Greater Yellowstone Ecosystem, *Limnol.*
 754 *Oceanogr.*, 44(3), 668–682, doi: 10.4319/lo.1999.44.3.0668.

755 Itaki, T., and Ikehara, K., (2004), Middle to late Holocene changes of the Okhotsk Sea
 756 Intermediate Water and their relation to atmospheric circulation, *Geophys. Res. Lett.*, 31,
 757 L24309, doi: 10.1029/2004GL021384.

758 Jones, V.J., Leng, M.J., Solovieva, N., Sloane, H.J. and Tarasov, P., (2004) Holocene climate
 759 of the Kola Peninsula; evidence from the oxygen isotope record of diatom silica, *Quat. Sci.*
 760 *Rev.*, 23(7–8), 833–839, doi: 10.1016/j.quascirev.2003.06.014.

761 Jones, M. C., Wooller, M., and Peteet, D.M., (2014), A deglacial and Holocene record of
 762 climate variability in south-central Alaska from stable oxygen isotopes and plant macrofossils
 763 in peat, *Quat. Sci. Rev.*, 87, 1–11, doi: 10.1016/j.quascirev.2013.12.025.

764 Juggins, S., (2014), C2 Data Analysis. Version 1.7.6. University of Newcastle, Newcastle.

765 Kalnay, E. *et al.* (1996), The NCEP/NCAR 40-Year Reanalysis Project. *Bull. Am. Meteorol.*
 766 *Soc.*, 77, 437–471.

767 Kaufman, D.S., Ager, T.A., Anderson, N.J., Anderson, P.M., Andrews, J.T., Bartelein, P.J.,
 768 Burbaker, L.B., Coats, L.L., Cwynar, L.C., Duval, M.L., Dyke, A.S., Edwards, M.E., Eiser,
 769 W.R., Gajewski, K., Geisodottir, A., Hu, F.S., Jennings, A.E., Kaplan, M.R., Kewin, M.W.,
 770 Lozhkin, A.V., MacDonald, G.M., Miller, G.H., Mock, C.J., Oswald, W.W., Otto-Blisner,
 771 B.L., Porinchu, D.F., Rühland, K., Smol, J.P., Steig, E.J., and Wolfe, B.B., (2004), Holocene
 772 thermal maximum in the western Arctic (0-180° W), *Quat. Sci. Rev.*, 23, 529–560, doi:
 773 10.1016/j.quascirev.2003.09.007.

774 Kaufman, D.S., Axford, Y.L., Henderson, A.C.G., McKay, N.P., Oswald, W.W., Saenger, C.,
 775 Anderson, R.S., Bailey, H.L., Clegg, B., Gajewski, K., Sheng Hu, F., Jones, M.C., Massa, C.
 776 Routson, C.C., Werner, A., Wooller, M.J., and Yu, Z., (2016), Holocene climate changes in
 777 eastern Beringia (NW North America) — A systematic review of multi-proxy evidence,
 778 *Quat. Sci. Rev.*, 147, 312–339, doi: 10.1016/j.quascirev.2015.10.021.

779 Krammer, K., and Lange-Bertalot, H., (1986–1991), *Bacillariophyceae Band 2/2*. Gustav
780 Fischer Verlag, Stuttgart, pp.1–4.

781 Krawiec, A.C.L, and Kaufman, D.S., (2014), Holocene storminess inferred from sediments of
782 two lakes on Adak Island, Alaska, *Quaternary Res.*, 82, 73–84, doi:
783 10.1016/j.yqres.2014.02.007.

784 Krawiec, A.C.L, Kaufman, D.S., and Vaillencourt, D.A., (2013), Age models and
785 tephrostratigraphy from two lakes on Adak Island, Alaska. *Quat. Geochronol.*, 18, 41–53,
786 doi: 10.1016/j.quageo.2013.07.002.

787 Labeyrie, L.D., (1974), New approach to surface seawater palaeotemperatures using $^{18}\text{O}/^{16}\text{O}$
788 ratios in silica of diatom frustules, *Nature*, 248, 40–42, doi: 10.1038/248040a0.

789 Lachniet, M.S., Lawson, D.E., Stephen, H., Sloat, A.R., and Patterson, W.P., (2016),
790 Isoscapes of $\delta^{18}\text{O}$ and $\delta^2\text{H}$ reveal climatic forcings on Alaska and Yukon precipitation, *Water*
791 *Resour. Res.*, 52(8), 6575–6586, doi: 10.1002/2016WR019436.

792 Lamb, A.L., Brewer, T.S., Leng, M.J., Sloane, H.J., and Lamb, H.F., (2007), A geochemical
793 method for removing the effect of tephra on lake diatom oxygen isotope records, *J.*
794 *Paleolimnol.*, 37, 499–516, doi: 10.1007/s10933-006-9034-5.

795 Larsen, C.F., Burgess, E., Arendt, A.A., O'neel, S., Johnson, A.J. and Kienholz, C., (2015),
796 Surface melt dominates Alaska glacier mass balance, *Geophys. Res. Lett.*, 42(14),
797 5902–5908, doi: 10.1002/2015GL064349. .

798 Leclerc, A.J., and Labeyrie, L., (1987), Temperature dependence of the oxygen isotopic
799 fractionation between diatom silica and water, *Earth Planet. Sci. Lett.*, 84(1), 69–74, doi:
800 10.1016/0012-821X(87)90177-4.

801 Leng, M.J., and Barker, P.A., (2006), A review of the oxygen isotope composition of
802 lacustrine diatom silica for paleoclimate reconstruction, *Earth Sci. Rev.*, 75, 5–27, doi:
803 10.1016/j.earscirev.2005.10.001.

804 Leng, M.J., and Sloane, H.J., (2008), Combined oxygen and silicon isotope analysis of
805 biogenic silica, *J. Quat. Sci.*, 23, 313–319, doi: 10.1002/jqs.1177.

806 Leng, M., Barker, P., Greenwood, P., Roberts, N., and Reed, J., (2001), Oxygen isotope
807 analysis of diatom silica and authigenic calcite from Lake Pinarbasi, Turkey, *J. Paleolimnol.*,
808 25(3), 343–349, doi: 10.1023/A:1011169832093.

809 Lepskaya, E.V., Jewson, D.H., and Usoltseva, M.V., (2010), *Aulacoseira subarctica* in
810 Kurilskoye Lake, Kamchatka: a deep, oligotrophic lake and important Pacific salmon
811 nursery, *Diatom Research*, 25(2), 323–335, doi: 10.1080/0269249X.2010.9705853.

812 Lotter, A.F., and Bigler, C., (2000), Do diatoms in the Swiss Alps reflect the length of
813 ice-cover? *Aquatic Sciences*, 62(2), 125–141, doi: 10.1007/s000270050002.

814 Lotter, A.F., Pienitz, R., and Schmidt, R., (2010), *Diatoms as indicators of environmental*
815 *change in subarctic and alpine regions*, In: Smol, J.P., Stoermer, E.F. (Eds.), *The Diatoms:*
816 *Application for the Environmental and Earth Sciences*. Cambridge University Press,
817 Cambridge.

818 Mackay, A.W., Swann, G.E.A., Brewer, T.S., Leng, M.J., Morley, D.W., Piotrowska, N.,
819 Rioual, P., and White, D., (2011), A reassessment of late glacial—Holocene diatom oxygen
820 isotope record from Lake Baikal using a geochemical mass-balance approach, *J. Quat. Sci.*
821 26, 627–634, doi: 10.1002/jqs.1484.

822 Mantua, N.J., Hare, S.R., Zhang, Y., Wallace, J.M., and Francis, R.C., (1997), A Pacific
823 interdecadal climate oscillation with impacts on salmon production, *Bull. Am. Meteorol. Soc.*,
824 78, 1069–1079, doi: 10.1175/1520-0477(1997)078<1069:APICOW>2.0.CO;2.

825 Marcott, S.A., Shakun, J.D., Clark, P.U., and Mix, A.C., (2013), A reconstruction of regional
826 and global temperature for the past 11 300 years, *Science*, 339, 1198–1201, doi:
827 10.1126/science.1228026.

828 Max, L., Riethdorf, J-R., Tiedemann R., Smirnova, M., Lembke-Jene, L., Fahl, K., Nürnberg,
829 D., Matul, A., and Mollenhauer, G., (2012), Sea surface temperature variability and sea-ice
830 extent in the subarctic northwest Pacific during the past 15,000 years, *Paleoceanography*, 27,
831 PA3213, doi:10.1029/2012PA002292.

832 Mayewski, P.A., Rohling, E.E., Stager, J.C., Karlén, K.A., Maasch, W., Meeker, L.D.,
833 Meyerson, E.A., Gasse, F., van Kreveld, S., Holmgren, K., Lee-Thorp, J., Rosqvist, G., Rack,
834 F., Staubwasser, M., Schneider, R.R., and Steiger, E.J., (2004), Holocene climate variability,
835 *Qual. Res.*, 62, 243–255, doi: 10.1016/j.yqres.2004.07.001.

836 Meyer, H., Chapligin, B., Hoff, U., Nazarova, L., and Diekmann, B., (2015), Oxygen isotope
837 composition of diatoms as Late Holocene climate proxy at Two-Yurts-Lake, Central
838 Kamchatka, Russia. *Glob. Planet. Chang.*, 134, 118–128, doi:
839 10.1016/j.gloplacha.2014.04.008.

840 Minoshima, K., Kawahata, H., and Ikehara, K., (2007), Changes in biological production in
841 the mixed water region (MWR) of the northwestern North Pacific during the last 27 kyr,
842 *Palaeogeogr. Palaeoclimatol. Palaeoecol.*, 254, 430–447, doi:10.1016/j.palaeo.2007.06.022.

843 Mock, C. J., Bartlein, P. J., and Anderson, P. M., (1998), Atmospheric circulation patterns
844 and spatial climatic variations in Beringia, *Int. J. Climatol.*, 10, 1085–1104,
845 doi:10.1002/(SICI)1097-0088(199808)18:10<1085::AID-JOC305>3.0.CO;2-K.

846 Morley, D.W., Leng, M.J., Mackay, A.W., Sloane, H.J., Rioual, P. and Battarbee, R.W.,
847 (2004), Cleaning of lake sediment samples for diatom oxygen isotope analysis, *J.*
848 *Paleolimnol.*, 31(3), 391–401, doi: 10.1023/B:JOPL.0000021854.70714.6b.

849 Nazarova, L., de Hoog, V., Hoff, U., Dirksen, O., and Diekmann, B., (2013), Late Holocene
850 climate and environmental changes in Kamchatka inferred from the subfossil chironomid
851 record, *Quat. Sci. Rev.*, 67, 81–92, doi: 10.1016/j.quascirev.2013.01.018.

852 NOAA, (2017), National Oceanic and Atmospheric Administration. National Climatic Data
853 Centre. <https://www.ncdc.noaa.gov/land-based-station-data>.

854 Rehfeld, K., Münch, T., Ho, S.L., and Laepple, T., (2018), Global patterns of declining
855 temperature variability from the Last Glacial Maximum to the Holocene, *Nature*, 554 (7692),
856 356–359, doi:10.1038/nature25454.

857 Renssen, H., Seppä, H., Heiri, O., Goosse, H., and Fichefet, T., (2009), The spatial and
858 temporal complexity of the Holocene thermal maximum, *Nat. Geosci.*, 2, 411–414, doi:
859 10.1038/ngeo513.

860 Renssen, H., Seppä, H., Crosta, X., Goosse, H., and Roche, D.M., (2012), Global
861 characterization of the Holocene Thermal Maximum, *Quat. Sci. Rev.*, 48, 7–19, doi:
862 10.1016/j.quascirev.2012.05.022.

863 Rioual, P., Andrieu-Ponel, V., Rietti-Shati, M., Battarbee, R.W., de Beaulieu, J.L., Cheddadi,
864 R., Reille, M., Svobodova, H., and Shemesh, A., (2001), High-resolution record of climate
865 stability in France during the last interglacial period, *Nature*, 413(6853), 293–296, doi:
866 10.1038/35095037.

867 Rioual, P., Andrieu-Ponel, V., de Beaulieu, J.L., Reille, M., Svobodova, H., and Battarbee,
868 R.W., (2007), Diatom responses to limnological and climatic changes at Ribains Maar

869 (French Massif Central) during the Eemian and Early Würm, *Quat. Sci. Rev.*, 26(11),
870 1557–1609, doi: 10.1016/j.quascirev.2007.03.009.

871 Roberts, S., Jones, V.J., Allen, J.R., and Huntley, B., (2015), Diatom response to mid-
872 Holocene climate in three small Arctic lakes in northernmost Finnmark, *The Holocene*, 25(6),
873 911–920, doi: 10.1177/0959683615572853.

874 Rodionov, S. N., Bond, N.A., and Overland, J.E., (2007), The Aleutian Low, storm tracks,
875 and winter climate variability in the Bering Sea, *Deep Sea Res. II.*, 54, 2560–2577, doi:
876 10.1016/j.dsr2.2007.08.002.

877 Rosqvist, G., Jonsson, C., Yam, R., Karlén, W., and Shemesh, A., (2004), Diatom oxygen
878 isotopes in pro-glacial lake sediments from northern Sweden: a 5000 year record of
879 atmospheric circulation, *Quat. Sci. Rev.*, 23(7), 851–859, doi:
880 10.1016/j.quascirev.2003.06.009.

881 Rühland, K., Priesnitz, A., and Smol, J.P., (2003), Paleolimnological evidence from diatoms
882 for recent environmental changes in 50 lakes across Canadian Arctic treeline, *Arct. Antarct.*
883 *Alp. Res.*, 35(1), 110–123, doi: 10.1657/1523-0430(2003)035[0110:PEFDFR]2.0.CO;2.

884 Rühland, K., Paterson, A.M., and Smol, J.P., (2008), Hemispheric-scale patterns of
885 climate-related shifts in planktonic diatoms from North American and European lakes, *Glob.*
886 *Change Biol.*, 14(11), 2740–2754, doi: 10.1111/j.1365-2486.2008.01670.x.

887 Saros, J.E. and Anderson, N.J., 2015. The ecology of the planktonic diatom *Cyclotella* and its
888 implications for global environmental change studies, *Biol. Rev.*, 90(2), 522–541, doi:
889 10.1111/brv.12120.

890 Savoskul, O.S., (1999), Holocene glacier advances in the headwaters of Sredniaya Avacha,
891 Kamchatka, Russia, *Qual. Res.*, 52, 14–26, doi: 10.1006/qres.1999.2051.

892 Schiff, C.J., Kaufman, D.S., Wolfe, A.P., Dodd, J., and Sharp, Z., (2009), Late Holocene
893 storm-trajectory changes inferred from the oxygen isotope composition of lake diatoms, south
894 Alaska, *J. Paleolimnol.*, 41, 189–208, doi: 10.1007/s10933-008-9261-z.

895 Smol, J. P., Wolfe, A. P., Birks, H. J. B., Douglas, M. S., Jones, V. J., Korhola, A., Pienitz,
896 R., Rühland, K., Sorvari, S., Antoniades, D., and Brooks, S. J., (2005), Climate-driven regime
897 shifts in the biological communities of arctic lakes., *PNAS*, 102(12), 4397–4402, doi:
898 10.1073/pnas.0500245102.

899 Solomina, O.N., Bradley, R.S., Hodgson, D.A., Ivy-Ochs, S., Jomelli, V., Macintosh, A.N.,
900 Nesje, A., Owen, L.A., Wanner, H., Wiles, G.C., and Young, N.E., (2015), Holocene glacier
901 fluctuations, *Quat. Sci. Rev.*, 111, 9–34, doi: 10.1016/j.quascirev.2014.11.018.

902 Solovieva, N., Klimaschewski, A., Self, A. E., Jones, V. J., Andrén, E., Andreev, A. A.,
903 Hammarlund, D., Lepskaya, E.V., and Nazarova, L., (2015), The Holocene environmental
904 history of a small coastal lake on the north-eastern Kamchatka Peninsula, *Glob. Planet.*
905 *Change*, 134, 55–66, doi: 10.1016/j.gloplacha.2015.06.010.

906 Spaulding, S.A., Lubinski, D.J. and Potapova, M., (2017), Diatoms of the United States.
907 <http://westerndiatoms.colorado.edu>

908 Streletskiy, D.A., Tananaev, N.I., Opel, T., Shiklomanov, N.I., Nyland, K.E., Streletskaya,
909 I.D. and Shiklomanov, A.I., (2015), Permafrost hydrology in changing climatic conditions:
910 seasonal variability of stable isotope composition in rivers in discontinuous permafrost.
911 *Environ. Res. Lett.*, 10 (9), p.095003, doi: 10.1088/1748-9326/10/9/095003.

912 Sundqvist, H.S., Kaufman, D.S., McKay, N.P., Balascio, N.L., Briner, J.P., Cwynar, L.C.,
913 Sejrup, H.P., Seppä, H., Subetto, D.A., Andrews, J.T. and Axford, Y., (2014), Arctic
914 Holocene proxy climate database—new approaches to assessing geochronological accuracy

915 and encoding climate variables *Clim. Past*, 10(4), 1605–1631, doi: 10.5194/cp-10-1605-
 916 2014.

917 Swann, G.E.A., and Patwardhan, S.V., (2011), Application of Fourier Transform Infrared
 918 Spectroscopy (FTIR) for assessing biogenic silica sample purity in geochemical analyses and
 919 palaeoenvironmental research, *Clim. Past*, 7, 65–74, doi: 10.5194/cp-7-65-2011.

920 TDX (2013), TDX Power - Adak Reconnaissance Study. *Hatch*.
 921 <http://akenergyinventory.org/hyd/SSH-2013-0004.pdf>

922 ter Braak, C.J.F., and Prentice, I.C., (1988), A theory of gradient analysis, *Adv. Ecol. Res.*,
 923 18, 271–317, doi: 10.1016/S0065-2504(03)34003-6.

924 Trenberth, K.E., and Hurrell, J.W., (1994), Decadal atmosphere-ocean variations in the
 925 Pacific, *Clim. Dyn.*, 9, 303–319, doi: 10.1007/BF00204745.

926 USGS, (2017), USGS *Landsat* 8 Images. Available at: <https://landsat.gsfc.nasa.gov/>

927 Vachula, R.S., Chipman, M.L., and Hu, F.S., (2017), Holocene climatic change in the
 928 Alaskan Arctic as inferred from oxygen-isotope and lake-sediment analyses at Wahoo Lake,
 929 *The Holocene*, 27 (4), 1–14, doi: <https://doi.org/10.1177/0959683617702230>.

930 Walker, M., Berhelhammer, M., Björck, S., Cwynar, L.C., Fisher, D.A., Long, A.J., Lowe,
 931 J.J., Newnham, R.M., Rasmussen, S.O., and Weis, H., (2012), Formal subdivision of the
 932 Holocene Series/Epoch: a discussion Paper by a Working Group of INTIMATE (Integration
 933 of ice-core, marine and terrestrial records) and the Subcommittee on Quaternary
 934 Stratigraphy (International Commission on Stratigraphy), *J. Quat. Sci.*, 27, 649–659, doi:
 935 10.1002/jqs.2565.

936 Wang, L., Lu, H., Liu, J., Gu, Z., Mingram, J., Chu, G., Li, J., Rioual, P., Negendank, J.F.,
 937 Han, J., and Liu, T., (2008), Diatom-based inference of variations in the strength of Asian

938 winter monsoon winds between 17,500 and 6000 calendar years BP, *J. Geophys. Res. Atmos.*,
939 113, D2101, doi: 10.1029/2008JD010145.

940 Welker, J.M., (2000), Isotopic ($\delta^{18}\text{O}$) characteristics of weekly precipitation collected
941 across the USA: an initial analysis with application to water source studies, *Hydrol.*
942 *Process.*, 14(8), 1449–1464, doi: 10.1002/1099-1085(20000615)14:8<1449::AID-
943 HYP993>3.0.CO;2-7.

944 Wiles, G., D'Arrigo, R., Villalba, R., Calkin, P., and Barclay, D.J., (2004), Century-scale
945 solar variability and Alaskan temperature change over the past millennium, *Geophys.*
946 *Res. Lett.* 31, L15203, doi: 10.1029/2004GL020050.

947 Zander, P.D., Kaufman, D.S., Kuehn, S.C., Wallace, K.L., and Anderson, R.S., (2013), Early
948 and late Holocene glacial fluctuations and tephrostratigraphy, Cabin Lake, Alaska, *J. Quat.*
949 *Sci.*, 28, 761–771, doi: 10.1002/jqs.2671

950 Zhang, Y., Renssen, H., Seppä, H., and Valdes, P.J., (2017), Holocene temperature
951 evolution in the Northern Hemisphere high latitudes—Model-data comparisons, *Quat. Sci.*
952 *Rev.*, 173, 101–113, doi: 10.1016/j.quascirev.2017.07.018.

953 **Author contributions**

954 D.S.K was PI, led the fieldwork and retrieved the sediment cores. D.S.K., H.L.B, H.J.S.,
955 A.C.G.H. and M.J.L developed the study concept. H.L.B conducted the research, sample
956 preparation, SEM, diatom and statistical analyses, interpreted the results, produced the
957 figures, and wrote the original manuscript. D.S.K. and A.L.H. critically revised the original
958 manuscript, and together with H.M. and J.M.W. provided technical advice and comments.
959 H.J.S performed the FTIR and diatom isotope measurements. M.J.L. supervised the diatom
960 isotope measurements and undertook the isotope corrections. H.J.S., A.C.G.H., M.J.L., H.M.
961 and J.M.W provided minor editorial revisions. All authors approved the final manuscript.

The authors declare no competing financial interests.

Figure captions

FIG1.JPG [Image size: 1.5 page width]

Figure 1. Location of (a) Adak Island in the central Aleutian Islands, (b) Heart Lake and Andrew Lake, (c) oblique north west view of Heart Lake with the inflow channel visible in the foreground [credit: Yarrow Axford], and (d) monthly mean precipitation (blue bars) and surface air temperature at Adak airport (1949–2016), whereby solid lines depict mean (black), minimum (blue) and maximum (red) temperatures [NOAA, 2017]. Numbered circles in 1a indicate key sites referred to in text: (1) LV29-114-3 [Max *et al.* 2012], (2) Pechora Lake [Hammarlund *et al.* 2015], (3) SO201-12-77KL [Max *et al.* 2012], (4) Horse Trail Fen [Jones *et al.* 2014], (5) Mica Lake [Schiff *et al.* 2009], (6) Mount Logan [Fisher *et al.* 2008], and (7) Jellybean Lake [Anderson *et al.* 2005]

FIG2.JPG [Image size: Column width]

Figure 2. Mean winter (December–February) sea level pressure associated with the six most positive (a) and negative (b) North Pacific Index (NPI) values between 1950 and 2017 [Trenberth and Hurrell, 1994]. A negative (positive) NPI is a strong (weak) Aleutian Low. Arrows highlight the direction of the primary storm tracks delivering precipitation to our site on Adak Island (yellow star) [Bailey *et al.* 2015]. SLP data obtained from NCEP/NCAR V1 reanalysis [Kalnay *et al.* 1996]. Numbered yellow circles in (a) indicate locations of the (1) LV29-114-3 [Max *et al.* 2012], (2) Pechora Lake [Hammarlund *et al.* 2015], (3) SO201-12-77KL [Max *et al.* 2012], (4) Horse Trail Fen [Jones *et al.* 2014], (5) Mica Lake [Schiff *et al.* 2009], (6) Mount Logan [Fisher *et al.* 2008], and (7) Jellybean Lake [Anderson *et al.* 2005] climate records discussed in text

988

989 **FIG3.PDF** [Image size: Full page width]

990 Figure 3. Heart Lake diatom stratigraphy and Principal Components Analysis (PCA) scores
991 of the 11 dominant diatom species (>5 % abundance), grouped by habitat preference. Diatom
992 zone demarcation (dashed lines 1–4) is guided by the CONISS cluster analysis. Variables are
993 plotted on a linear timescale (ka BP) and the depth scale refers to depth below lake floor

994

995 **FIG4.PDF** [Image size: Column width]

996 Figure 4. Loadings of the 11 dominant diatom taxa from Heart Lake and their corresponding
997 PCA scores. Sample scores (circles) are coloured according to their down core diatom
998 assemblage Zone (1–4). Dashed coloured ellipses group diatom species by their habitat
999 preference

1000

1001 **FIG5.PDF** [Image size: Full page width]

1002 Figure 5. Time series of Heart Lake $\delta^{18}\text{O}_{\text{diatom}}$ during (a) the past millennium and (b) the
1003 Holocene. Horizontal dashed grey lines indicate the Holocene and the 21st century mean
1004 $\delta^{18}\text{O}_{\text{diatom}}$ value. Orange diamonds and white triangles indicate previously published
1005 radiocarbon ages and tephra beds, respectively [Krawiec *et al.* 2013]. Vertical blue bars
1006 correspond to three intervals of Little Ice Age glacier advance in mainland Alaska [Solomina
1007 *et al.* 2015]

1008

1009 **FIG6.PDF** [Image size: Column width]

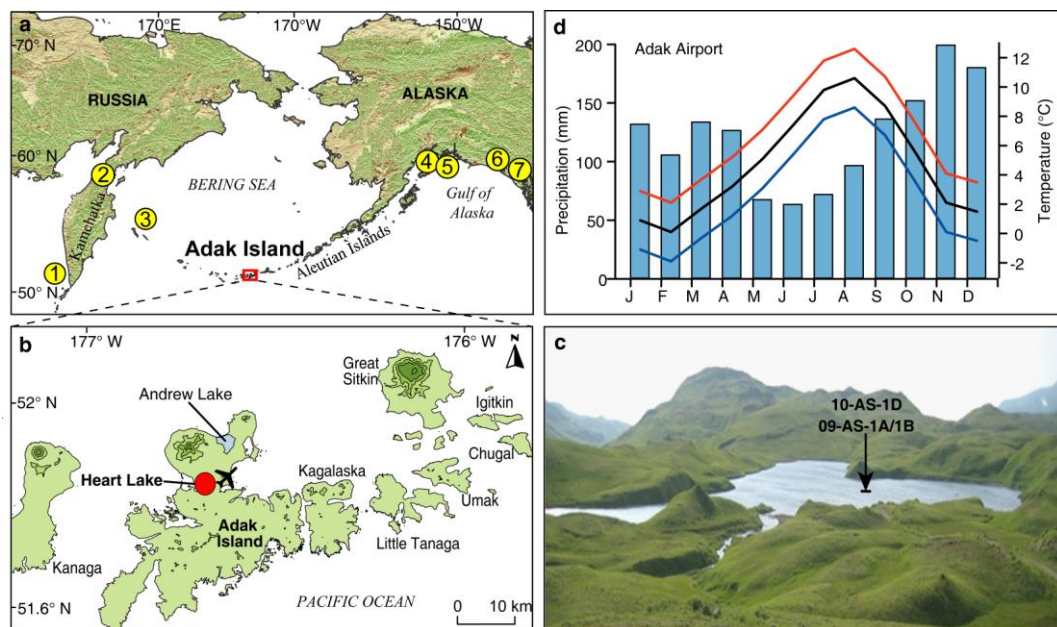
1010 Figure 6. Heart Lake bottom water $\delta^{18}\text{O}$ (2009 and 2010) on the local meteoric water line
1011 (LMWL) and the global meteoric water line (GMWL). LMWL data are derived from Adak
1012 monthly composite precipitation samples collected by the Global Network of Isotopes in
1013 Precipitation (GNIP) [IAEA/WMO, 2017]

FIG7.PDF [Image size: Column width]

Figure 7. Holocene time series of (a) summer (JJA) insolation at 65°N [Berger and Loutre, 1991], (b) alkenone SSTs from LV29-114-3 in the Okhotsk Sea [Max et al. 2012], (c) Pechora Lake $\delta^{18}\text{O}$ [Hammarlund et al. 2015], (d) Heart Lake $\delta^{18}\text{O}_{\text{diatom}}$ (this record), (e) intervals of expanded mountain glaciers in eastern Beringia [Solomina et al. 2015], (f) Mica Lake $\delta^{18}\text{O}$ [Schiff et al. 2009], (g) Mount Logan ice $\delta^{18}\text{O}$ [Fisher et al. 2008], (h) Horse Trail Fen $\delta^{18}\text{O}$ [Jones et al. 2014], and (i) Jellybean Lake $\delta^{18}\text{O}$ [Anderson et al. 2005]. Black lines in (g) and (i) represent 40-yr smoothed intervals. Vertical red shading indicates the eastern Beringia mid-Holocene Thermal Maximum [Kaufman et al. 2016], blue shading indicates the Little Ice Age (LIA) [Solomina et al. 2015]

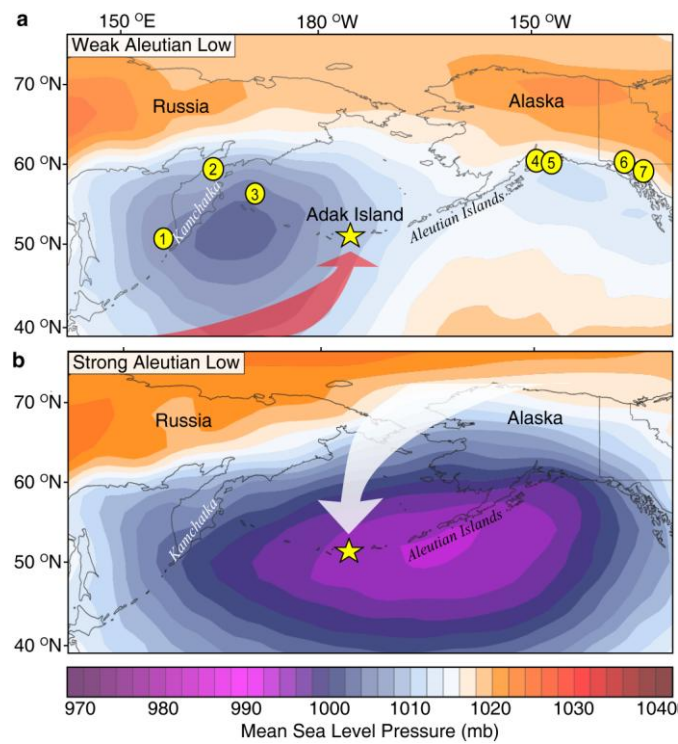
Figures

FIG1



1032

FIG2



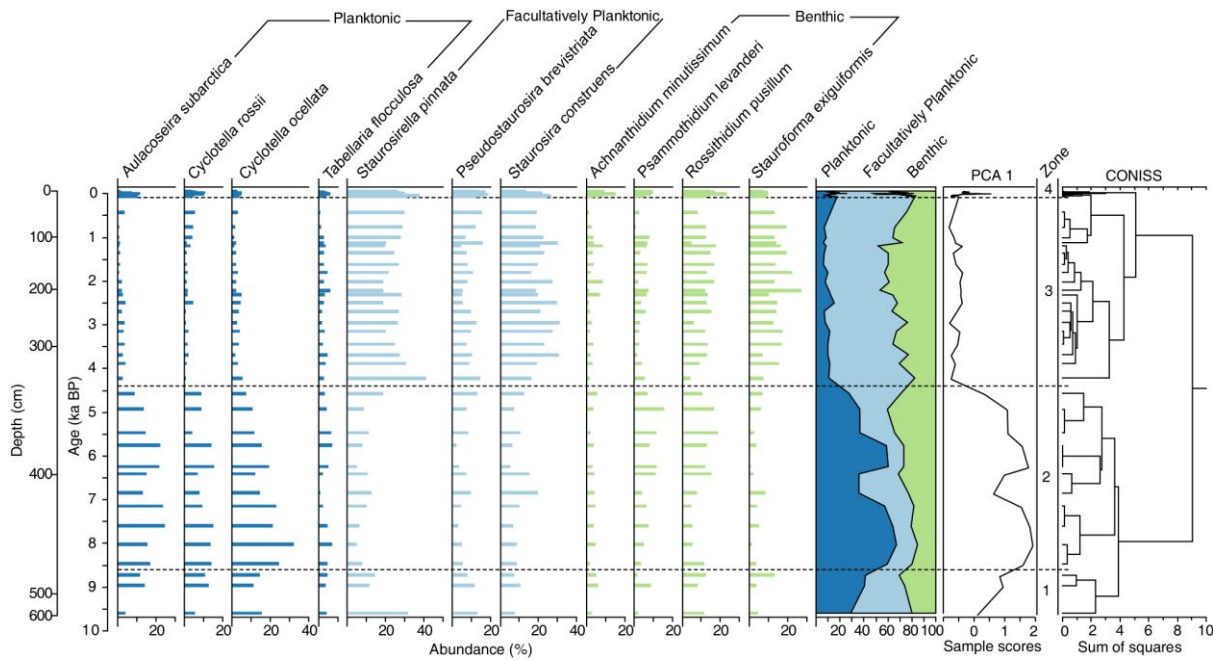
1033

1034

1035

1036

FIG3



1037

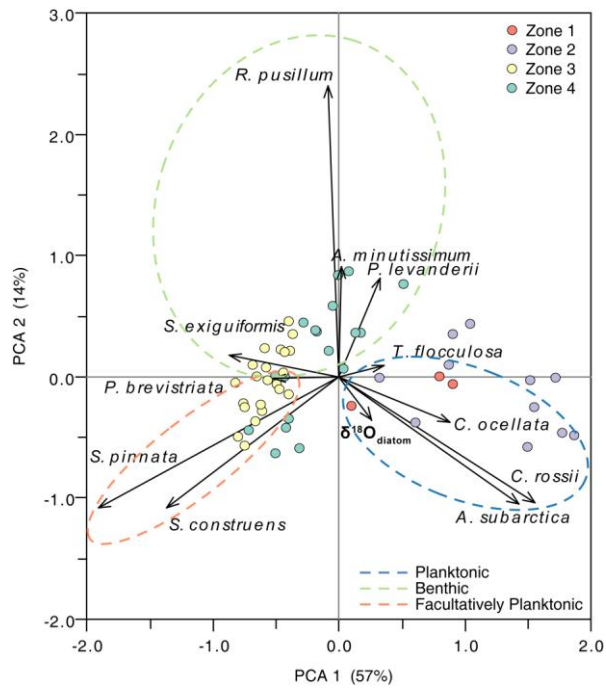
1038

1039

1040

1041

FIG4

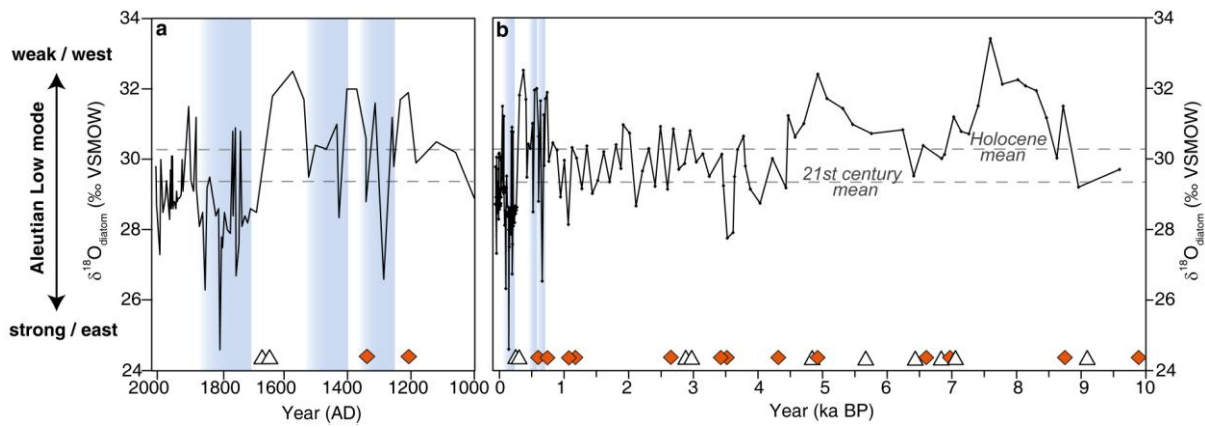


1042

1043

1044

FIG5



1045

1046

1047

1048

1049

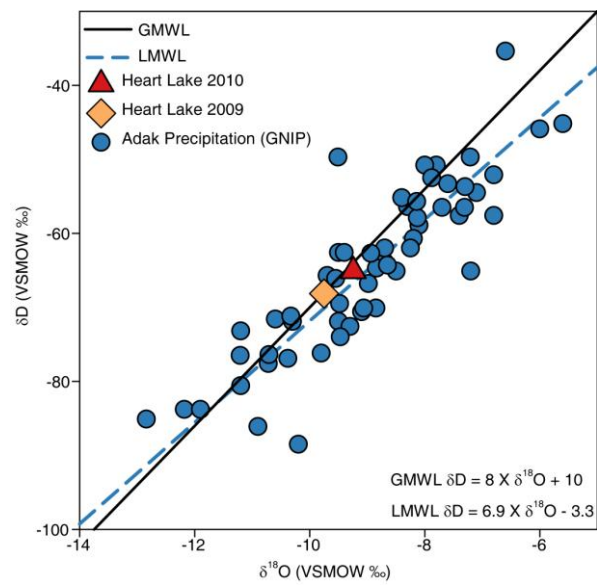
1050

1051

1052

1053

FIG6



1054

1055

FIG7

